Journal of Materials Chemistry C

ROYAL SOCIETY OF CHEMISTRY

PAPER

View Article Online
View Journal | View Issue

Cite this: J. Mater. Chem. C, 2023, 11, 8961

Understanding enormous redshifts in highly concentrated Mn^{2+} phosphors†

Arnoldus J. van Bunningen,* Simon Tobias Keizer and Andries Meijerink *

Received 3rd March 2023,
Accepted 25th May 2023

DOI: 10.1039/d3tc00778b

rsc.li/materials-c

Broad band near infrared (NIR) emission has recently been reported for a wide variety of concentrated Mn^{2+} phosphors. Typically, Mn^{2+} emits in the green to red spectral region, depending on local coordination. The enormous redshift to the NIR was explained by exchange coupling between Mn^{2+} neighbours at high Mn^{2+} dopant concentrations. However, the reported redshifts are an order of magnitude larger than expected for exchange coupling and also the absence of a shift in excitation spectra suggests that exchange coupling cannot explain the observations. Here, extensive concentration, temperature and time dependent luminescence studies are reported for $Mg_{1-x}Mn_xAl_2O_4$ (x = 0.01–0.5). The results show that the broad band NIR emission originates from NIR emitting trap centers, possibly Mn^{3+}. High Mn^{2+} dopant concentrations enable efficient energy migration over the Mn^{2+} sublattice to these traps, consistent with the same excitation spectra for the green Mn^{2+} and NIR trap emission. Upon cooling to cryogenic temperatures energy migration is hampered and the green Mn^{2+} emission increases, especially in the most concentrated systems. Finally, the relative intensity of the NIR emission was varied by changing synthesis conditions providing further support that the NIR emission in concentrated Mn^{2+} phosphors originates from NIR emitting centers and not exchange coupled Mn^{2+} pairs.

Introduction

The development of new luminescent materials (phosphors) is crucial for improving white light LEDs for lighting and displays and also for enabling new applications. Important current topics in the LED phosphor industry concern narrow band red and green phosphors to improve the light quality, colour gamut and efficacy.[1–5] New applications are emerging and include human centric lighting and lighting for horticulture.[6–11] An interesting spectral region is the near infrared (NIR). In addition to applications in horticulture (controlling plant growth) and human centric lighting (adding NIR to the lamp spectrum for health benefits), NIR emitters are now gaining attention for chemical sensing.[12,13] For both narrow band phosphors and NIR emitters there is increasing interest in phosphors relying on the luminescence of the Mn^{2+} ion.[14,15]

Mn^{2+} has a long history of applications in a variety of phosphors for lighting and displays.[16,17] The luminescence properties of Mn^{2+} are versatile and can be understood based on the Tanabe–Sugano diagram for the $3d^5$ configuration. Mn^{2+} typically yields narrow band green emission in tetrahedral coordination and red emission in octahedral coordination resulting from the $^4T_1 \rightarrow {}^6A_1$ transition. The luminescence quenching temperature can be very high, making Mn^{2+} phosphors attractive for applications where high temperatures are reached, *e.g.* in white light LEDs (wLEDs).[18] Drawbacks are the weak absorption ($\varepsilon < 1\ M^{-1}\ cm^{-1}$) and long luminescence life time ($\tau >$ ms) as all transitions within the $3d^5$ configuration are spin- and parity forbidden. The weak absorption can be mitigated by combining Mn^{2+} with a strongly absorbing sensitizer and the emission life time can be shortened by incorporation in a host lattice with heavier elements (stronger spin–orbit coupling) or through magnetic interactions, *e.g.* in Mn^{2+} pairs (partially lifting the spin selection rule).[19–25] In the past decade a new emission was reported for Mn^{2+}: NIR emission from exchange coupled Mn^{2+}-pairs.[25–34] This broad band NIR emission was observed in a variety highly doped Mn^{2+} phosphors and deemed promising for applications in both lighting and sensing.

Before considering these recent findings of NIR emission in highly-doped Mn^{2+} phosphors, it is good to discuss early work on the optical properties of exchange-coupled Mn^{2+} pairs. In an insightful review in 1988 McCarthy and Güdel summarize experimental findings and theoretical explanations for the role of exchange coupling in redshifting the Mn^{2+} emission and shortening the emission life time.[20] The spectral shifts are determined by the exchange coupling parameter J in the ground state and J_{ex} in the excited state. Depending on distance, geometry and bridging ligands, values for J and J_{ex} vary and are typically tens of cm^{-1}. The redshift and shortening of

Debye Institute for Nanomaterials Science, Utrecht University, 3584 CC Utrecht, The Netherlands. E-mail: A.J.vanBunningen@uu.nl, A.Meijerink@uu.nl

† Electronic supplementary information (ESI) available. See DOI: https://doi.org/10.1039/d3tc00778b

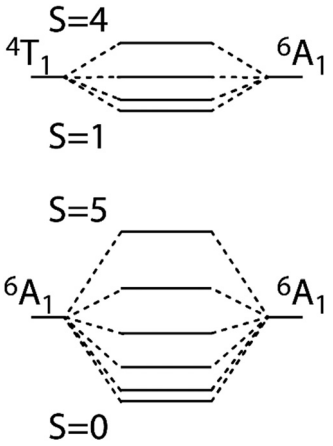

Fig. 1 Schematic of exchange coupling between Mn^{2+} neighbours in the $^6A_1$ ground state (S = 5/2) giving rise to total spin S varying from 0 to 5 while exchange coupling with one ion in the $^4T_1$ excited state (S = 3/2) gives rise to total spin S varying from 1 to 4.[20,21] In case of antiferromagnetic interaction S = 0 is the lowest state while for ferromagnetic interaction S = 5 will be the ground state for the exchange coupled pair. Note that the actual exchange splitting is much smaller than the splitting in the schematic figure.

decay time are explained using an energy level diagram (Fig. 1) in which the total spin for the pair in the ground state can vary from 0 to 5 (with steps of 1) depending on the relative orientation of the S = 5/2 spins of the exchange coupled Mn^{2+} ions and of the S = 5/2 and S = 3/2 spins for the pair with one ion in the excited state. The total spin magnetic moments for the pair can thus be 0, 1, 2, 3, 4 or 5 in the ground state and 1, 2, 3 or 4 in the excited state, giving rise to partially spin-allowed transitions between pair states with the same total spin. In the review several examples of exchange coupled pairs are discussed, showing redshifts of typically 10–100 cm^{-1}, for example for Mn^{2+} pairs in $CsMgCl_3$, $KMgF_3$ and for Cr^{3+} pairs in ruby (Al_2O_3:Cr^{3+}).[20,21,36,37] For several commercial phosphors the concentration dependent redshift was later also experimentally observed, theoretically explained and related to phosphor performance. In the famous green willemite phosphor Zn_2SiO_4:Mn^{2+} the emission maximum shifts from 520 to 529 nm ($\sim$250 cm^{-1}) upon raising the concentration from 0.5 to 20% Mn^{2+}.[38,39] In the electroluminescent ZnS:Mn^{2+} phosphor similar Mn-concentration dependent shifts are observed as well NIR emission.[40,41] The NIR emission was explained by energy migration to NIR emitting centers of which the nature was not known. In an overview of luminescence properties of exchange coupled pairs of transition metal (TM) ions in 2001 also Mn^{2+}–Mn^{2+} pairs were discussed and a spectral shift from 519 to 528 nm accompanied by life time shortening from 7.2 to 4.5 ms was reported for $MgAl_2O_4$ doped with 0.2 to 10% Mn^{2+}.[21] Even though not all aspects of exchange coupling can be quantitatively explained, the influence of exchange coupling on the Mn^{2+} (and other TM ions) luminescence properties are well documented.

In the past decade unexpected NIR emission for heavily doped Mn^{2+} phosphors was reported for a wide variety of materials, including $KZnF_3$, $MgGa_2O_4$, MnS, CaO, $MgAl_2O_4$, $CsMnF_3$, $(Gd,Y)_3(Ga,Al)_5O_{12}$ and Li_2ZnSiO_4.[26–35] In 2014 the first papers reported a strongly redshifted NIR emission band in addition to the 'normal' Mn^{2+} emission in $KZnF_3$ and $MgGa_2O_4$.[26,27] In $KZnF_3$ the normal 585 nm emission intensity decreased upon raising the Mn^{2+} concentration above 10% and a strong NIR emission at 770 nm appeared. Similar observations in $MgGa_2O_4$ revealed green emission shifting from 507 to 518 nm for Mn^{2+} concentrations of 1 to 20%. This green emission intensity strongly decreased upon raising the Mn^{2+} concentration and was accompanied by a strong increase of a broad 770 nm NIR emission band, gaining intensity for Mn^{2+} concentrations above 10%. In both cases the visible Mn^{2+} emission was assigned to the $^4T_1 \rightarrow {}^6A_1$ transition on isolated Mn^{2+} while the NIR emission band was assigned to exchange coupled Mn^{2+} pairs, in the case of $KZnF_3$ Mn^{2+} in adjacent octahedral sites and in the case of $MgGa_2O_4$ to Mn^{2+} ions in edge-sharing neighbouring tetrahedral and octahedral sites. The exchange coupling theory, as outlined in ref. 19, 20, 41 was cited to explain the redshift. In the years following many more examples were reported and included in reviews on Mn^{2+} doped phosphors. For example, in MnS deep red emission at 710 nm was assigned to isolated Mn^{2+} and two NIR 900 and 1380 nm emission bands were explained by emission from next-nearest and nearest neighbour exchange coupled pairs.[28] DFT calculations were done to support similar assignments in CaO:Mn^{2+}.[29] In a recent paper a difference in thermal quenching behavior of the two emission bands in heavily Mn-doped Li_2ZnSiO_4 was used for temperature sensing.[34]

The vast number of papers and host lattices showing broad band NIR emission at high Mn^{2+} doping concentrations seems convincing but the redshifts reported for the exchange-coupled Mn^{2+} pairs are very large, varying from 3400 cm^{-1} in $(Gd,Y)_3(Ga,Al)_5O_{12}$ and Li_2ZnSiO_4 to 6800 cm^{-1} in $MgAl_2O_4$ and MnS.[28,32] These shifts are more than ten times larger than those reported in earlier work,[20,21,36,37,40,42,43] where clear evidence was presented for the magnitude of the exchange splitting parameters J and J_{ex} based on temperature dependent luminescence and decay measurements as well as experiments in magnetic fields. In fact, the small shifts of the visible emission bands of Mn^{2+} upon raising the concentrations (*e.g.* from 507 to 518 nm in $MgGa_2O_4$) are consistent with earlier results on redshifts expected for exchange coupled Mn^{2+} pairs. In addition, no large shifts are observed in the excitation spectra which is unexpected for high concentrations of exchange coupled Mn-pairs with a strongly distorted energy level scheme that would be expected based on the enormous redshifts reported for the emission. It is the aim of this work resolve the discrepancies between the recent papers and earlier work on exchange coupled Mn-pairs.

To find the origin for the NIR emission in heavily Mn^{2+} doped phosphors, here the luminescence properties of $Mg_{1-x}Al_2O_4$:Mn_x (x = 0.01 to 0.5) are investigated in detail. The $MgAl_2O_4$:Mn^{2+} phosphor is well studied and serves as a model system to provide insight. As Mn^{2+} doping is raised, a prominent NIR emission appears, consistent with the results reported in.[32] However at low temperatures ($<$100 K), this NIR emission decreases, while the typical green emission of Mn^{2+} ($^4T_1 \rightarrow {}^6A_1$) reappears. In addition, the relative intensity of the NIR

emission is shown to depend on synthesis conditions and host stoichiometry. Based on our experimental findings, we propose a different origin for the NIR emission: it does not originate from exchange coupled Mn^{2+} pairs but from NIR emitting traps. At high doping concentrations efficient energy migration between excited Mn^{2+} ions facilitates energy transfer to this NIR luminescent center, which we tentatively assign to trace amounts of Mn^{3+}. Energy migration is hampered at cryogenic temperatures, explaining the reappearance of the green Mn^{2+} emission. Synthesis conditions favoring incorporation of Mn^{3+} result in a higher NIR emission intensity and are consistent with our assignment.

Methods

For the synthesis of microcrystalline $Mg_{1-x}Mn_xAl_2O_4$ the starting materials MgO (99.99%,Sigma Aldrich), Al_2O_3 (99.99%,chempur), and $MnCO_3$ (99.99%,Sigma Aldrich) were mixed in stoichiometric amounts in an agate mortar and pestle. The mixture was wetted with a few drops of acetone (to prevent microparticle aggregation), and ground manually for 15 minutes. The mixtures were then annealed twice in a tube oven for a total of 18 h at 1500 °C in a reducing atmosphere (H_2/N_2 20/80) and were reground in between.

The powders were examined using powder X-ray powder diffraction for phase purity. A Phillips PW1729 X-ray generator, Cu Kα source was used at 40 kV operating voltage and 20 mA current. The step size resolution was 0.02° 2θ. Photoluminescence (PL) spectroscopy was performed using an Edinburgh Instruments FLS-920 fluorescence spectrometer. The photoluminescence (PL) and PL excitation (PLE) measurements were recorded using a 450 W Xe lamp as excitation source and a Hamamatsu R928 PMT or a Hamamatsu N7422 PMT detector for the visible and NIR spectral region, respectively. To properly compare the intensity of the NIR with the VIS detector the spectra were normalised on the 650–700 nm peaks that were measured with both detectors. Spectra are corrected for the instrumental response. PL decay measurement were performed by using a tuneable optical paramagnetic oscillator (OPO) Opotek Opolette HE 355II pulsed laser (pulse width: 10 ns; repetition rate: 20 Hz) as excitation source and the Hamamatsu R928 PMT combined with the Multi Channel Scaling (MCS) time resolved measuring card in the Edinburgh spectrometer (10 μs time resolution). For temperature dependent measurements a liquid He cooled cryostat from Oxford Instruments was used.

Results and discussion

Concentration dependent luminescence

To investigate the concentration dependent luminescence properties of $Mg_{1-x}Mn_xAl_2O_4$, a series of samples was made under identical synthesis conditions with x = 0.01, 0.02, 0.05, 0.1, 0.2 and 0.5. The materials came out of the tube oven as white powder for low-doped samples while at high doping concentrations ($x > 0.10$) the body color was slightly yellowish. XRD powder diffraction confirmed that all samples were phase pure (ESI† Fig. S1). The diffraction angles showed a continuous decrease for increasing Mn content as expected based on Vegard's law and the fact that the ionic radius of Mn^{2+} is larger than that of Mg^{2+} and thus the crystal unit cell expands upon increasing Mn-content. Note that in the $MgAl_2O_4$ host it is expected that Mn^{2+} mainly occupies the Mg^{2+} site (similar size, same charge) creating a tetrahedrally coordinated Mn.[44] Mn^{2+} emission has also been reported for Mn^{2+} on the Al^{3+} site in $Mg_{1-x}Mn_xAl_2O_4$.[45]

To characterize the Mn^{2+} luminescence for isolated Mn^{2+} ions, first PL and PLE spectra were recorded for $MgAl_2O_4$ doped with 1% Mn. In Fig. 2 the PL spectrum is shown. Narrow band green emission peaking at 520 nm is observed, consistent with earlier reports. The emission band is assigned to the $^4T_1 \rightarrow {}^6A_1$ transition on Mn^{2+}. In addition there is a very weak sharp emission line at 680 nm. This is typical for Cr^{3+} at the Al^{3+} site and careful measurement of the position of the $^2E \rightarrow {}^4A_2$ zero-phonon line and vibronic structure show that these are identical to what has been reported for Cr^{3+} in $MgAl_2O_4$ providing evidence for the incorporation of a small amount of Cr^{3+} in our materials.[46] Cr is a common contaminant in the Al_2O_3 precursor. The recorded PLE spectrum of the green Mn^{2+} emission shows six distinct peaks, at 280, 350, 380, 425, 450 and 480 nm. These are all d–d transitions of the Mn^{2+} and can be assigned to transitions from the $^6A_1$ ground state to the $^4A_2(^4F)$, $^4E(^4D)$, $^4T_2(^4D)$, $^4A_1/E(^4G)$, $^4T_2(^4G)$ and $^4T_1(^4G)$ excited states, respectively. No broad emission around 650 nm is observed. Emission at this wavelength is typical for Mn^{2+} at the octahedral Al site.[45]

The concentration dependence of the luminescence was investigated by measuring luminescence spectra for all Mn^{2+} concentrations over a wide spectral range, extending to 1200 nm. Note that in the past NIR emissions from highly Mn-doped samples may have been missed because of low sensitivity of detectors (photomultipliers) in the NIR. In Fig. 3 the emission spectra are shown. The green 520 nm emission band increases in intensity up to 5% Mn^{2+} followed by a decrease above 10%. For the highest concentrations, 20 and 50% Mn^{2+}, the green emission is almost completely quenched. The emission maximum shifts from 518 to 526 nm upon raising the Mn^{2+} concentration from 1 to 50%. In the concentration region where

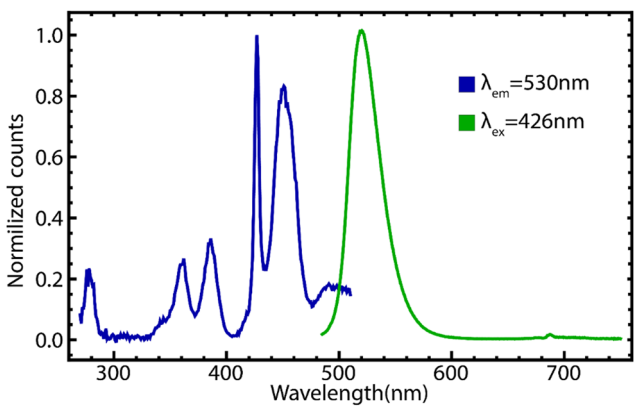

Fig. 2 Photoluminescence (green) and excitation (blue) spectrum of $Mg_{0.99}Mn_{0.01}Al_2O_4$ at 300 K. The PL spectrum was recorded under 426 nm excitation, the PLE spectrum for 530 nm emission.

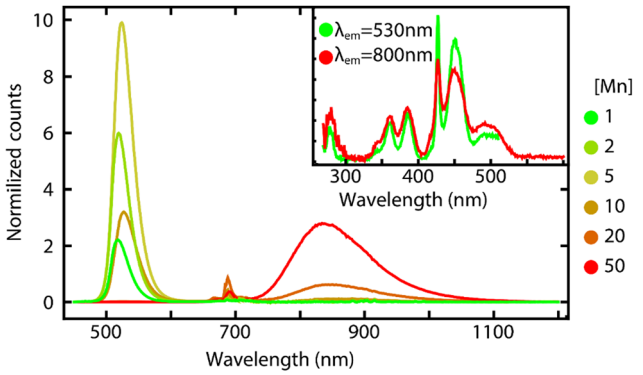

Fig. 3 Emission spectra of $Mg_{1-x}Mn_xAl_2O_4$ for x = 0.01,0.02,0.05,-0.10,0.20,0.50, excited at 425 nm. From 450 to 800 nm the spectra were measured with a R928 detector and in the NIR region (600 to 1200 nm) with a N7422 detector. The peak at ~680 nm was used to scale the spectra. The inset shows the excitation spectrum of the green emission of the 1% Mn and of the NIR emission of the 50% Mn material.

the green emission is quenched, a NIR emission band around 830 nm is observed to increase with Mn-dopant concentration. The highest NIR intensity is found for the 50% dopant concentration. The present results are in good agreement with the trends observed for the visible and NIR emission in other host lattices where the NIR emission was assigned to exchange coupled Mn-pairs. Specifically, the spectra and relative intensities of visible and NIR emission are also consistent with results reported for concentration dependent Mn^{2+} luminescence in $MgAl_2O_4$.[21,32]

In the inset of Fig. 3, the excitation spectra of the green emission for the 1% Mn and the NIR emission in 50% doped $MgAl_2O_4$ are shown. The excitation spectra are similar and the assignment to Mn^{2+} d–d transition as discussed above can explain the features. The peak positions are almost identical while the excitation bands are broadened for the 50% doped host. The broadening can be explained by inhomogeneous broadening. The disorder in the Mg/Mn sublattice is maximized in the 50/50% material and will give rise to variations in the local crystal field splitting, induced by the difference in ionic radii for Mn and Mg. Variations in the local Mn–Mg distribution over nearest and possibly next-nearest neighbour lattice sites will thus give rise in differences in the crystal field splitting for Mn^{2+} and disorder is maximized in the host lattice with 50% Mn^{2+}.

To further investigate the origin of the NIR emission band, luminescence decay curves were recorded for both the green and NIR emission as a function of concentration following pulsed excitation (~10 ns pulse duration) at 420 nm. Excited state dynamics can give valuable information on the role of energy transfer processes. The results in Fig. 4(a) for the green emission show that for 1 and 2% Mn the decay curves are close to single exponential with a decay time of 6.1 ms for 1 and 2% and drops to 0.5 ms at 20% Mn. The 6.1 ms is in agreement with decay times reported for 1–2% Mn^{2+}-doped samples in ref. 21 For concentrations of 5% and higher the decay becomes faster and increasingly non-exponential which can be explained by shortening of the life time by exchange coupling and, especially for higher Mn^{2+} concentrations, energy migration and transfer to trap centers. The decay curves for the NIR emission in Fig. 4(b) also show decay on a ms time scale. The decay curves are non-exponential and decay times decrease for higher Mn^{2+} concentrations. The similar decay behavior observed for the NIR and green emission (non-exponential with an average decay time in the ms range) can be expected when the trap emission is populated by transfer from Mn^{2+} ions and the decay profile of the trap emission reflects the decrease in population of Mn^{2+} that feeds the trap states.

Based on the concentration dependent luminescence measurements an alternative explanation for the NIR emission band can be given. Upon increasing dopant concentrations above 10% resonant energy transfer between Mn^{2+} dopant ions leads to concentration quenching. Due to the efficient energy transfer between neighbouring Mn^{2+} ions the excited state probes a larger volume and even in case of low concentrations of trapping sites, efficient energy transfer to trap states can occur. Especially above the percolation point (the concentration at which a 3D connected network of dopants is formed) efficient energy migration to traps occurs, leading to quenching of the dopant emission and, in the case of luminescent traps, a strong increase in trap emission. This phenomenon is well-known in the field of luminescent materials.[47–49] The concentration dependent luminescence properties for $MgAl_2O_4$:Mn are consistent with this model: above 10% Mn^{2+} the NIR trap emission intensity rapidly increases while the green Mn^{2+} emission drops. The luminescence decay time of the Mn^{2+} donor decreases by migration mediated energy transfer to the trap states. The excitation spectrum for the

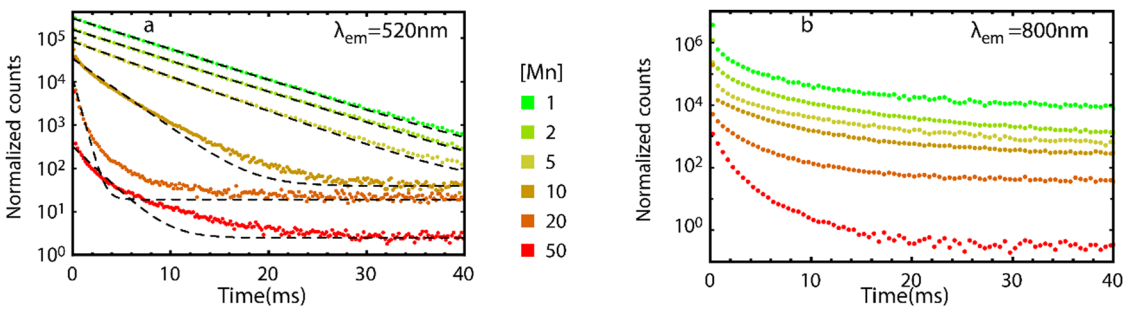

Fig. 4 Luminescence decay curves of Mn^{2+} in $Mg_{1-x}Al_2O_4$:Mn_x (x = 0.01,0.02,0.05,0.10,0.20,0.50) for pulsed λ_{ex} = 427 nm excitation (curves are offset for clarity). (a) Decay curves for λ_{em} = 520 nm, the dashed lines show the fit assuming mono exponential decay. (b) Decay curves for λ_{em} = 830 nm.

trap emission is identical to that of the Mn^{2+} ions as the concentration of (and thus direct absorption by) the traps is very low. Following absorption by Mn^{2+} efficient transfer feeds the NIR emitting traps and this explains why the excitation spectrum for the NIR trap emission coincides with the Mn^{2+} absorption spectrum.

Note that in the earlier explanation (green emission from isolated Mn^{2+}, NIR emission from exchange coupled Mn^{2+} pairs) there is no clear explanation for the fast drop in decay time for the green emission. Isolated Mn^{2+} is expected to have a long ms decay time while the exchange coupled Mn-pairs have a faster decay by partial lifting of the selection rules. Also the similarity in excitation spectra is unexpected for the model in which the NIR emission is explained by exchange coupled Mn-pairs. Strong exchange coupling is required to explain the large redshift in emission and this large change in energy level structure should then also be reflected in changes in absorption transition energies. This is not observed. In other reports where strongly redshifted emission in concentrated Mn^{2+} phosphors is reported[26–35] also no corresponding significant change in the excitation or absorption spectra is observed while it would be expected for such strong exchange coupling. Only for γ-MnS an additional 606 nm excitation band appeared in the excitation spectrum of the NIR but this can be due to direct excitation of the NIR emitting centers.[28]

Temperature dependent luminescence

To further elucidate the nature of the NIR emission in highly doped Mn^{2+} luminescent materials, temperature dependent measurements can help. Energy migration involves many consecutive energy transfer steps between neighbouring Mn^{2+} ions. Small variations in local environment give rise to small energy differences between the $^4T_1$ excited state of different Mn^{2+} ions. At room temperature these small energy differences can be easily compensated by absorption or emission of phonons, making resonant energy transfer possible. However, upon cooling to cryogenic temperatures, the excitation energy will be trapped at Mn^{2+} ions which have their $^4T_1$ excited state at lower energies. Further transfer to a Mn^{2+} neighbour with a higher energy $^4T_1$ state would require absorption of a phonon which is not available as the phonons are frozen out a cryogenic temperatures. Extensive research on energy migration for especially lanthanide ions has beautifully demonstrated how at low temperatures energy migration is hampered and emission from perturbed lanthanide ions is observed as a slightly red shifted sharp line emission.[50,51] Interestingly, also for concentrated Mn^{2+} thermally activated energy migration to NIR emitting trap centers has been reported.[52]

To investigate the role of energy migration in feeding the NIR emission in $Mg_{1-x}Mn_xAl_2O_4$ temperature dependent emission spectra down to cryogenic temperatures were performed for the $MgAl_2O_4$:50% Mn sample. The emission spectra are shown in Fig. 5. Upon cooling to 100 K there are no large changes but below 100 K a rapid increase in the green emission intensity observed while the NIR emission intensity decreases. The inset in Fig. 5 shows the integrated emission intensities of

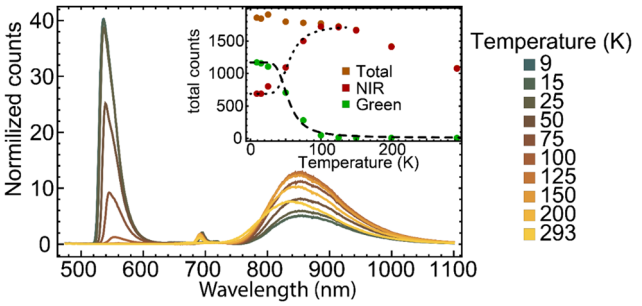

Fig. 5 Temperature dependent emission spectra of $MgAl_2O_4$:50% Mn, λ_{ex} = 426 nm. The inset shows the integrated intensity of the green and NIR emission bands. The dashed line shows the fit to determine the activation energy (ΔE of 200 cm^{-1}) for energy migration. The dotted line is a visual guide to show that the NIR emission increases simultaneously with the decrease of the green emission.

the NIR and visible emission bands as a function of temperature, normalized to the intensity at 4 K. The temperature dependence is consistent with efficient energy migration over the Mn^{2+} sublattice at room temperature, feeding the NIR emitting traps, which is hampered upon cooling below 100 K. The NIR emission dominates above 100 K and shows a small decrease upon raising the temperature to 300 K, possibly by thermal quenching of the NIR luminescence.

To quantify the activation energy that is necessary to overcome these energy fluctuations an Arrhenius equation was used to fit the observed temperature dependence of green emission intensity, as shown with the dashed line in Fig. 5. An effective ΔE of 200 cm^{-1} was found. This value is consistent with what can be expected based on the broadening of the excitation bands for $Mg_{0.5}Mn_{0.5}Al_2O_4$ and also with earlier results by Güdel *et al.* on MnF_2 single crystals where it was shown that perturbations by Ca impurities could lower the energy levels of nearby Mn^{2+} ions by 250 cm^{-1}.[53] In Fig. 6 the temperature dependent energy transfer is schematically depicted. At room temperature (Fig. 6(b)) efficient energy transfer between Mn^{2+} neighbours allows for rapid energy migration to NIR emitting trap centers resulting in dominant NIR emission for concentrations above the percolation point where an interconnected 3D network of Mn^{2+} ions is formed. At cryogenic temperatures (Fig. 6(a)) small energy differences between neighbouring Mn^{2+} ions hamper energy migration and result in a strong enhancement of the green Mn^{2+} emission.

The observed temperature dependence of the green and NIR emission is not consistent with the assignment of the green emission to isolated Mn^{2+} ions and the NIR emission to exchange coupled pairs. The concentration of isolated ions and exchange coupled pairs does not change with temperature and thus the strong increase of the green emission upon cooling from 100 K to 4 K cannot be explained by a model in which the green emission results from isolated ions and the NIR emission from exchange coupled pairs, especially for high Mn-doping concentrations where almost all Mn^{2+} ions are expected to be in pairs. A similar temperature dependence was previously even reported for fully concentrated Mn-system (*e.g.* MnS and $CsMnF_3$) where

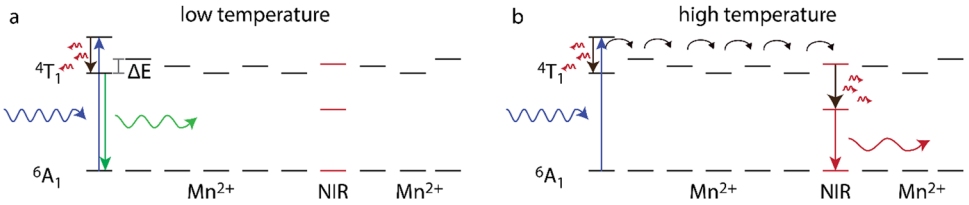

Fig. 6 Schematic illustration of energy migration to NIR emitting trap centers. (a) At low temperature energy migration is hampered by the lack of thermal energy to bridge energy differences leading to trapping the excitation energy at Mn^{2+} sites with slightly lower $^4T_1$ state resulting in an enhanced green Mn^{2+} emission and reduced NIR trap emission. (b) Energy migration to NIR emitting centers at room temperature where the small energy differences of the $^4T_1$ states for neighbouring Mn^{2+} ions can be thermally overcome by lattice vibrations leading to dominant NIR emission.

the isolated Mn^{2+} visible emission appeared upon cooling to 10 K. Clearly in a fully concentrated Mn^{2+} system all Mn^{2+} ions are in pairs and no isolated Mn^{2+} ions exist. For the $CsMnF_3$ material the observation of isolated Mn^{2+} emission at low temperature was attributed to competition between antiferromagnetic and ferromagnetic coupling interaction while for MnS no explanation was given for the observation of isolated Mn^{2+} visible emission upon cooling. In the $MgAl_2O_4$ system the NIR pair emission was assigned to pairs of Mn^{2+} ions on 'normal' four-coordinated Mg sites and six-coordinated Al^{3+} sites. Analysis of EXAFS data was used to determine that for 5% or less Mn^{2+} doping all Mn^{2+} was on IV-coordinated sites and for 10% or more Mn^{2+} ~8–10% of Mn^{2+} ions occupied octahedral VI-coordinated sites. This can explain an increase of isolated Mn^{2+} emission upon cooling by hampering energy migration to Mn-pairs at cryogenic temperatures, similar to the energy migration to NIR trap centers discussed above. Unfortunately, the evidence for a significant Mn^{2+} concentration in octahedral sites is inconclusive. The EXAFS data show poor fits and most importantly, no red Mn^{2+} emission typical for Mn^{2+} on octahedral sites can be observed for any Mn^{2+} concentration.

The temperature dependence of luminescence decay curves for the green and NIR emission in $MgAl_2O_4$:50% Mn is shown in Fig. 7. At low temperatures (<50 K) the decay curves are characterized by a single exponential tail and a fast initial decay. This shape is characteristic of single step energy transfer and limited or no energy migration. One-step energy transfer to the NIR emitting centers gives rise to faster initial decay for those Mn^{2+} ions close to a NIR center and the single exponential tail (with decay times longer than 6 ms) reflects the radiative decay for Mn^{2+} ions which are not in proximity to a NIR emitting center. Above ~50 K the decay in the tail becomes faster indicating an onset of energy migration that becomes faster as the temperature is raised and results in more efficient energy transfer to NIR centers through energy migration, depopulating the green emitting excited states. The temperature dependence of the NIR emission is more complex. It is on time scales similar to the decay of the green emission, indicating that the observed decay dynamics are controlled by the feeding states, in agreement with energy migration from Mn^{2+} to the NIR emitting centers.

Influence of non-stoichiometry

The results and discussion presented above provide strong evidence that the broad NIR emission originates from trap centers. Excitation of Mn^{2+} and energy migration over the Mn^{2+} sublattice is followed by efficient energy transfer to the NIR emitting center. A candidate for the NIR center is Mn^{3+}. It is known that Mn^{3+} can show efficient NIR emission[52,54–57] in the 700–1000 nm spectral region and the 3+ valence state is a well-known for Mn. The broad band Red/NIR emission from Mn^{3+} is typically assigned to the $^1T_2 \rightarrow {}^5E$ emission but may also originate from the $^5T_2 \rightarrow {}^5E$ transition. To investigate if the NIR emitter is Mn^{3+}, non-stoichiometric samples doped with 10%Mn were synthesized while varying the amounts of MgO and Al_2O_3 precursor. It can be expected that excess Al_2O_3 will reduce the concentration of Mn^{3+} and that excess MgO will increase the Mn^{3+} concentration, based on the following equilibria reactions[58]:

$$3MgO \leftrightharpoons 2Mg'_{Al} + Mg^{\times}_{Mg} + 3O^{\times}_{O} + V^{\bullet\bullet}_{O}$$

$$3Al_2O_3 + V^{\bullet\bullet}_{O} \leftrightharpoons 4Al^{\times}_{Al} + 2Al^{\bullet}_{Mg} + 9O^{\times}_{O}$$

$$Mn^{\times}_{Mg} + V^{\bullet\bullet}_{O} \leftrightharpoons Mn'_{Mg} + V^{\bullet}_{O}$$

As Al is exclusively 3+ and Mg exclusively 2+, defect equilibria where is Mn is trivalent (either on a Mg^{2+} site or on a Al^{3+} site)

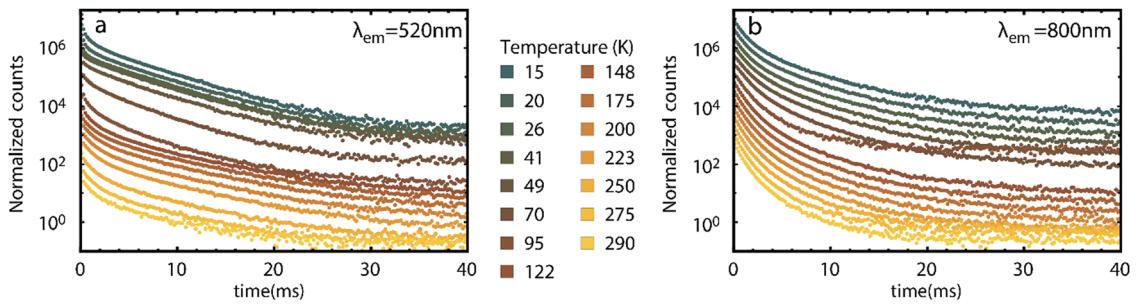

Fig. 7 Luminescence decay curves of the (a) 520 nm and (b) 800 nm emission in $MgAl_2O_4$:50% Mn following pulsed 427 nm excitation as a function of temperature.

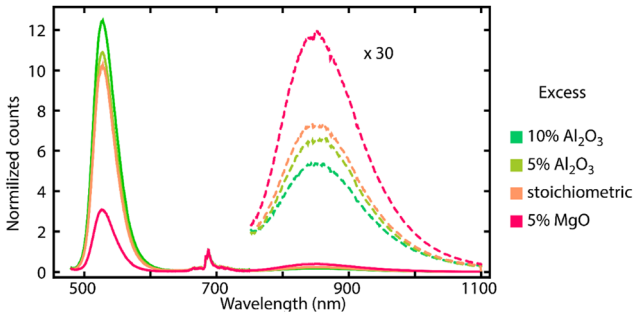

Fig. 8 Emission spectra of $MgAl_2O_4$:10% Mn synthesized with different excess of precursors. The NIR emission is also shown 30x enhanced for better visibility. The spectra were normalised at the 688 nm emission peak.

will be shifted towards lower Mn^{3+} concentration in the presence of excess Al^{3+} ions while excess Mg^{2+} will shift the equilibria towards more Mn^{3+}. The emission spectra in Fig. 8 show indeed a strong increase in the NIR emission for 5% excess MgO and a decrease for 5 or 10% excess Al_2O_3.

The assignment of the NIR emission to trivalent Mn^{3+} is in agreement with the experimental results. At higher dopant concentrations the strong increase in NIR emission is not only caused by enhanced energy migration over the Mn^{2+} sublattice but also, for a constant fraction of Mn being in the 3+ state, the absolute concentration of NIR emitting centers would increase at higher dopant concentrations giving rise to a sharp increase in NIR emission intensity for higher Mn-concentrations. Still, the identification of the NIR emitting trap as Mn^{3+} should be taken with some caution. NIR emission is also observed in undoped $MgAl_2O_4$[59] this suggests that the NIR emission could also be caused by an intrinsic defect. In a recent paper by Sun *et al.* NIR emission from Mn^{2+} was observed and in line with the present findings not assigned to exchange coupled pairs but to Mn^{2+} in dodecahedral sites.[60] It is notoriously difficult to unravel the nature of defects in luminescent materials and further research is needed to confirm the nature of the NIR emitting trap center for the many phosphors in which broad band NIR emission is observed at high Mn-doping concentrations and the nature of the NIR emitting trap center can vary for the different concentrated Mn^{2+} phosphors.

Discussion

The results and analysis presented above provide strong evidence that the enormous redshifts observed in concentrated Mn^{2+} phosphors do not originate from exchange coupled Mn^{2+} pairs. It is however important to realize that exchange interaction does affect the luminescence of transition metal ions, especially for spin-forbidden transitions. For Mn^{2+} much higher absorption strengths have been reported for Mn^{2+} pairs *e.g.* in $KMgF_3$, $CsMg_{0.95}Mn_{0.05}Cl_3$ and $CsMg_{0.80}Mn_{0.20}Br_3$.[61,62] In excitation and absorption spectra additional strong exchange coupled Mn^{2+}-pair bands appeared between 10 and 20 K as the $S = 1$ pair state was thermally populated (see Fig. 1) and the partially spin-allowed transition to the $S = 1$ excited became possible. The temperature range (10–20 K) and spectral shift of the pair absorption lines show that the exchange coupling strengths for Mn^{2+} are of the order of tens of cm^{-1}, consistent with theoretical calculations. In recent publications redshifted NIR emission was also reported for exchange coupled Cr^{3+} dimers with shifts of about 1000 cm^{-1} from the isolated $^2E \rightarrow {}^4A_2$ Cr^{3+} emission around 700 nm.[63,64] These shifts are in line with redshifts expected for exchange coupled Cr^{3+} pairs. Exchange interaction in dimers is known to be stronger for Cr^{3+} than for Mn^{2+} which results in higher magnetic transition temperatures (*e.g.* $T_N \sim 308$ K for Cr_2O_3[65] *vs.* 118 K for MnO[66]) and spectral shifts observed for exchange coupled pairs of Cr^{3+} ions are much larger than for Mn^{2+}. In the review by McCarthy and Güdel examples, including Cr^{3+} pairs in ruby, are discussed with spectral shifts of hundreds of cm^{-1} of the R-line emission for Cr^{3+} pairs.[20]

Exchange interaction in transition metal ions pairs can give rise to stronger absorption and shorter emission decay times by relaxing the spin-selection rule and spectral shifts that vary depending on host lattice and transition metal ion. This can be exploited in the emerging field of new phosphors for NIR LEDs. The reported enormous redshifts for Mn^{2+} exchange coupled pairs of up to 7000 cm^{-1} are however more than an order of magnitude larger than what can be expected for Mn^{2+} pairs and this, together with the absence of changes in the excitation spectra of the redshifted emission and the observation of a strong increase of normal Mn^{2+} emission in highly concentrated Mn^{2+} phosphors at cryogenic temperatures, warrants the conclusion that the enormous redshifts observed in the emission of concentrated Mn^{2+} phosphors does not originate from exchange coupled Mn^{2+} pairs but from NIR emitting trap centers.

Conclusions

The origin of the NIR emission in highly Mn-doped phosphors was investigated. Earlier reports assign the NIR emission to exchange coupled Mn^{2+}-pairs in variety of host lattices. The reported spectral shifts are however more than 10 times larger than what can be expected based on exchange coupling parameters for Mn^{2+}. Careful studies over a wide Mn-concentration range in $Mg_{1-x}Mn_xAl_2O_4$ (x = 0.01–0.5) indicate that energy migration towards NIR emitting trap centers is responsible for the NIR emission and not exchange coupled Mn-pairs. Temperature dependent measurement on $MgAl_2O_4$:50% Mn reveal a strong increase in the green emission intensity upon cooling to cryogenic temperatures, while the NIR emission intensity drops. This is consistent with energy migration that is hampered upon cooling as it requires thermal activation. The temperature dependence cannot be explained by a model in which exchange coupled Mn-pairs cause the NIR emission band in highly concentrated Mn-systems. Moreover, no redshifted absorption band is observed which would be expected for exchange coupled Mn-pairs. The NIR emitting center is tentatively assigned to Mn^{3+} and this assignment is supported by variations in the relative intensity of the NIR emission band in non-stoichiometric materials synthesized with excess MgO or Al_2O_3. Although the exact nature of the NIR

emitting center is difficult to pinpoint it is evident that exchange coupled Mn-pairs cannot be responsible for the strongly red-shifted emission in highly Mn-doped phosphors but that energy transfer to NIR emitting defects or impurities causes the NIR emission.

Conflicts of interest

There are no conflicts to declare.

Acknowledgements

Financial support from Nichia Corporation (Japan) is gratefully acknowledged.

References

1 Z. Xia and Q. Liu, Progress in discovery and structural design of color conversion phosphors for LEDs, *Prog. Mater. Sci.*, 2016, **84**, 59–117.
2 M. A. Van De Haar, M. Tachikirt, A. C. Berends, M. R. Krames, A. Meijerink and F. T. Rabouw, Saturation Mechanisms in Common LED Phosphors, *ACS Photonics*, 2021, **8**(6), 1784–1793.
3 E. Song, *et al.*, Highly Efficient and Stable Narrow-Band Red Phosphor Cs_2SiF_6:Mn^{4+} for High-Power Warm White LED Applications, *ACS Photonics*, 2017, **4**(10), 2556–2565.
4 G. J. Hoerder, *et al.*, $Sr[Li_2Al_2O_2N_2]$:Eu^{2+}—A high performance red phosphor to brighten the future, *Nat. Commun.*, 2019, **10**(1), 1824.
5 T. Senden, R. J. A. Van Dijk-Moes and A. Meijerink, Quenching of the red Mn^{4+} luminescence in Mn^{4+}-doped fluoride LED phosphors, *Light Sci. Appl.*, 2018, **7**(1), 2047–7538.
6 K. W. Houser and T. Esposito, Human-Centric Lighting: Foundational Considerations and a Five-Step Design Process, *Front. Neurol.*, 2021, **12**, 25.
7 S. Hariyani and J. Brgoch, Advancing Human-Centric LED Lighting Using Na_2MgPO_4F:Eu^{2+}, *ACS Appl. Mater. Interfaces*, 2021, **13**(14), 16669–16676.
8 S. Fang, T. Lang, M. Cai and T. Han, Light keys open locks of plant photoresponses: A review of phosphors for plant cultivation LEDs, *J. Alloys Compd.*, 2022, **902**, 163825.
9 X. Qiu, *et al.*, A far-red-emitting $(Gd,Y)_3(Ga,Al)_5O_{12}$:Mn^{2+} ceramic phosphor with enhanced thermal stability for plant cultivation, *J. Am. Ceram. Soc.*, 2020, **103**(9), 5157–5168.
10 M. C. Giménez, *et al.*, Effects of Near-Infrared Light on Well-Being and Health in Human Subjects with Mild Sleep-Related Complaints: A Double-Blind, Randomized, Placebo-Controlled Study, *Biology*, 2022, **12**(1), 60.
11 J. J. Casal, Shade Avoidance, *Arab. B.*, 2012, **10**, e0157.
12 J. Lai, *et al.*, Broadband near-infrared emitting from $Li_{1.6}Zn_{1.6}Sn_{2.8}O_8$:$Cr^{3+}$ phosphor by two-site occupation and Al^{3+} cationic regulation, *Mater. Des.*, 2020, **192**, 108701.
13 An introduction to near infrared (NIR) spectroscopy|IM Publications Open. Available: **https://www.impopen.com/introduction-near-infrared-nir-spectroscopy**. [Accessed: 08-Mar-2021].
14 Q. Zhou, *et al.*, Mn^{2+} and Mn^{4+} red phosphors: synthesis, luminescence and applications in WLEDs. A review, *J. Mater. Chem. C*, 2018, **6**(11), 2652–2671.
15 B. Su, G. Zhou, J. Huang, E. Song, A. Nag and Z. Xia, Mn^{2+}-Doped Metal Halide Perovskites: Structure, Photoluminescence, and Application, *Laser Photon. Rev.*, 2021, **15**(1), 2000334.
16 W. M. Yen, S. Shionoya and H. Yamamoto, *Phosphor Handbook*, CRC Press, 2018.
17 J. H. Schulman, Luminescence of $(Zn, Be)_2SiO_4$:Mn and other manganese-activated phosphors, *J. Appl. Phys.*, 1946, **17**(11), 902–908.
18 A. J. van Bunningen, A. D. Sontakke, R. van der Vliet, V. G. Spit and A. Meijerink, Luminescence Temperature Quenching in Mn^{2+} Phosphors, *Adv. Opt. Mater.*, 2023, 2202794.
19 A. D. Sontakke, A. J. Van Bunningen, F. T. Rabouw, S. Meijers and A. Meijerink, Unraveling the $Eu^{2+}\rightarrow Mn^{2+}$ Energy Transfer Mechanism in w-LED Phosphors, *J. Phys. Chem. C*, 2020, **124**(25), 13902–13911.
20 P. J. McCarthy and H. U. Güdel, Optical spectroscopy of exchange-coupled transition metal complexes, *Coord. Chem. Rev.*, 1988, **88**, 69–131.
21 A. P. Vink, M. A. de Bruin, S. Roke, P. S. Peijzel and A. Meijerink, Luminescence of Exchange Coupled Pairs of Transition Metal Ions, *J. Electrochem. Soc.*, 2001, **148**(7), E313.
22 J. Si, *et al.*, Structure, luminescence and energy transfer in Ce^{3+} and Mn^{2+} codoped γ-AlON phosphors, *J. Mater. Chem. C*, 2019, **7**(3), 733–742.
23 T. F. Soules, R. L. Bateman, R. A. Hewes and E. R. Kreidler, Energy Transfer between Antimony and Manganese in the Fluorophosphate Phosphors, *Phys. Rev. B: Solid State*, 1973, **7**(4), 1657.
24 H. Masai, *et al.*, High energy-transfer rate from Sn^{2+} to Mn^{2+} in phosphate glasses, *Opt. Mater. Express*, 2015, **5**(3), 617–622.
25 I. Matsuyama, N. Yamashita and K. Nakamura, Photoluminescence of the SrS:Mn^{2+} Phosphor and Pb^{2+}-Sensitized Luminescence of the SrS:Pb^{2+}, Mn^{2+} Phosphor, *J. Phys. Soc. Jpn.*, 2013, **58**(2), 741–751, DOI: **10.1143/JPSJ.58.741**.
26 E. Song, *et al.*, Anomalous NIR Luminescence in Mn^{2+}-Doped Fluoride Perovskite Nanocrystals, *Adv. Opt. Mater.*, 2014, **2**(7), 670–678.
27 E. H. Song, J. L. Wang, D. C. Yu, S. Ye and Q. Y. Zhang, Anomalous tunable visible to near infrared emission in the Mn^{2+}-doped spinel $MgGa_2O_4$ and room-temperature upconversion in the Mn^{2+} and Yb^{3+}-codoped spinel, *J. Mater. Chem. C*, 2014, **2**(41), 8811–8816.
28 Z. T. Chen, E. H. Song, M. Wu, B. Zhou and Q. Y. Zhang, Exchange coupled Mn-Mn pair: An approach for super-broadband 1380 nm emission in α-MnS, *Appl. Phys. Lett.*, 2016, **109**(19), 191907.
29 E. Song, *et al.*, Wavelength-Tunability and Multiband Emission from Single-Site Mn^{2+} Doped CaO Through Antiferromagnetic Coupling and Tailored Superexchange Reactions, *Adv. Opt. Mater.*, 2017, **5**(13), 1700070.

30 Z. Chen, E. Song, S. Ye and Q. Zhang, Tunable multiple emissions in manganese-concentrated sulfide through simultaneous tailoring of Mn-site coordination and Mn-Mn pair geometry, *J. Appl. Phys.*, 2017, **122**(21), 213102.
31 Z. Song, J. Zhao and Q. Liu, Luminescent perovskites: recent advances in theory and experiments, *Inorg. Chem. Front.*, 2019, **6**(11), 2969–3011.
32 E. Song, *et al.*, Heavy Mn^{2+} Doped $MgAl_2O_4$ Phosphor for High-Efficient Near-Infrared Light-Emitting Diode and the Night-Vision Application, *Adv. Opt. Mater.*, 2019, **7**(24), 1–9.
33 X. Zhu, *et al.*, Isolated-Mn^{2+}-like Luminescent Behavior in $CsMnF_3$ Caused by Competing Magnetic Interactions at Cryogenic Temperature, *J. Phys. Chem. C*, 2021, **125**(50), 27800–27809.
34 E. Song, *et al.*, Mn^{2+}-activated dual-wavelength emitting materials toward wearable optical fibre temperature sensor, *Nat. Commun.*, 2022, **13**(1), 1–9.
35 X. Feng, L. Lin, R. Duan, J. Qiu and S. Zhou, Transition metal ion activated near-infrared luminescent materials, *Prog. Mater. Sci.*, 2022, **129**, 100973.
36 J. Ferguson, H. U. Güdel, E. R. Krausz and H. J. Guggenheim, High resolution phosphorescence excitation spectroscopy of exchange coupled Mn^{2+} pairs in $KMgF_3$ and $KZnF_3$, *Mol. Phys.*, 1974, **28**(4), 893–904.
37 P. J. Mccarthy and H. U. Güdel, Contribution from the Optical Spectra of Exchange-Coupled Manganese(II) Pairs in Cesium Magnesium Trichloride and Cesium Magnesium Tribromide, *Inorg. Chem.*, 1984, **23**(7), 880–887.
38 C. R. Ronda and T. Amrein, Evidence for exchange-induced luminescence in Zn_2SiO_4: Mn, *J. Lumin.*, 1996, **69**(5–6), 245–248.
39 A. Morell and N. El Khiati, Green Phosphors for Large Plasma TV Screens, *J. Electrochem. Soc.*, 1993, **140**(7), 2019–2022.
40 C. Benecke, W. Busse, H. E. Gumlich and H. J. Moros, Evidence of different Mn luminescence centers in $Zn_{1-x}Mn_xS$ by time resolved laser spectroscopy, *J. Lumin.*, 1988, **40–41**(C), 627–628.
41 P. De Visschere, *et al.*, Analysis of the luminescent decay of ZnS:Mn electroluminescent thin films, *J. Lumin.*, 1995, **65**(4), 211–219.
42 L. R. Bradshaw, J. W. May, J. L. Dempsey, X. Li and D. R. Gamelin, Ferromagnetic excited-state Mn^{2+} dimers in $Zn_{1-x}Mn_xSe$ quantum dots observed by time -resolved magnetophotoluminescence, *Phys. Rev. B: Condens. Matter Mater. Phys.*, 2014, **89**(11), 115312.
43 J. Ferguson, H. U. Güdel, E. R. Krausz and H. J. Guggenheim, High resolution phosphorescence excitation spectroscopy of exchange coupled Mn^{2+} pairs in $KMgF_3$ and $KZnF_3$, *Mol. Phys.*, 1974, **28**(4), 893–904.
44 R. D. Shannon, Revised Effective Ionic Radii and Systematic Studies of Interatomie Distances in Halides and Chaleogenides, *Acta Crystallogr., Sect. A*, 1976, **32**, 751–767.
45 V. A. Dutov, *et al.*, Impurity Mn^{2+} defects in $MgAl_2O_4$ nanoceramics, *AIP Conf. Proc.*, 2020, **2313**(1), 030013.
46 A. Ćirić, Z. Ristić, J. Periša, Ž. Antić and M. D. Dramićanin, $MgAl_2O_4$:Cr^{3+} luminescence thermometry probe in the physiological temperatures range, *Ceram. Int.*, 2021, **47**(19), 27151–27156.
47 B. Henderson and G. F. Imbusch, *Optical spectroscopy of inorganic solids*, Oxford University Press, 2nd edn, 1989.
48 G. Blasse, Luminescence of inorganic solids: From isolated centres to concentrated systems, *Prog. Solid State Chem.*, 1988, **18**(2), 79–171.
49 G. Blasse and B. C. Grabmaier, *Luminescent Materials*, Springer-Verlag, Berlin, germany, 1994.
50 J. P. M. van Vliet, D. van der Voort and G. Blasse, Luminescence and energy migration in Eu^{3+}-containing scheelites with different anions, *J. Lumin.*, 1989, **42**(6), 305–316.
51 A. J. De Vries, M. F. Hazenkamp and G. Blasse, On the Gd^{3+} luminescence and energy migration in $Li(Y,Gd)F_4$–Tb^{3+}, *J. Lumin.*, 1988, **42**(5), 275–282.
52 O. Nijs, J. M. W. Verweij and G. Blasse, A divalent manganese garnet with red luminescence, *Mater. Chem. Phys.*, 1992, **30**(3), 199–203.
53 R. L. Greene, D. D. Sell and R. S. Feigelson, Impurity-Induced Optical Fluorescence in MnF_2, *Phys. Rev.*, 1968, **171**(2), 600–610.
54 S. Kück, S. Hartung, S. Hurling, K. Petermann and G. Huber, Emission of octahedrally coordinated Mn^{3+} in garnets, *Spectrochim. Acta, Part A*, 1998, **54**(11), 1741–1749.
55 L. Cornu, M. Duttine, M. Gaudon and V. Jubera, Luminescence switch of Mn-Doped $ZnAl_2O_4$ powder with temperature, *J. Mater. Chem. C*, 2014, **2**(44), 9512–9522.
56 L. Marciniak and K. Trejgis, Luminescence lifetime thermometry with Mn^{3+}–Mn^{4+} co-doped nanocrystals, *J. Mater. Chem. C*, 2018, **6**(26), 7092–7100.
57 K. Petermann and G. Huber, Broad band fluorescence of transition metal doped garnets and tungstates, *J. Lumin.*, 1984, **31–32**(PART 1), 71–77.
58 C. J. Ting and H. Y. Lu, Defect reactions and the controlling mechanism in the sintering of magnesium aluminate spinel, *J. Am. Ceram. Soc.*, 1999, **82**(4), 841–848.
59 N. Pathak, P. S. Ghosh, S. K. Gupta, S. Mukherjee, R. M. Kadam and A. Arya, An Insight into the Various Defects-Induced Emission in $MgAl_2O_4$ and Their Tunability with Phase Behavior: Combined Experimental and Theoretical Approach, *J. Phys. Chem. C*, 2016, **120**(7), 4016–4031.
60 Y. Xiao, W. Xiao, D. Wu, L. Guan, M. Luo and L.-D. Sun, An extra-broadband VIS-NIR emitting phosphor toward multifunctional LED applications, *Adv. Funct. Mater.*, 2022, **32**, 21009618.
61 J. Ferguson, H. U. Güdel, E. R. Krausz and H. J. Guggenheim, High -resolution phosphorescence excitation spectroscopy of exchange coupled Mn^{2+} pairs in $KMgF_3$ and $KZnF_3$, *Mol. Phys.*, 1974, **28**(4), 893–904.
62 P. J. McCarthy and H. U. Güdel, Optical spectra of exchange coupled manganese(II) pairs in cesium magnesium trichloride and cesium magnesium tribromide, *Inorg. Chem.*, 1984, **23**(7), 880–897.
63 V. Rajendran, M. H. Fang, W. T. Huang, N. Majewska, T. Lesniewski, S. Mahlik, G. Leniec, M. Kaczmarek,

W. K. Pang, V. K. Peterson, K. M. Lu, H. Chang and R. S. Liu, Chromium Ion Pair Luminescence: A Strategy in Broadband Near-Infrared Light-Emitting Diode Design, *J. Am. Ceram. Soc.*, 2021, **143**(45), 19058–19066.

64 V. Rajendran, K. C. Chen, W. T. Huang, M. Kaminski, M. Grzegorzyk, S. Mahlik, G. Leniec, K. M. Lu, D. H. Wei, H. Chang and R. S. Liu, Unraveling Luminescent Energy Transfer Pathways: Futuristic Approach of Miniature Shortwave Infrared Light-Emitting Diode Design, *ACS Energy Lett.*, 2023, **8**(5), 2395–2400.

65 S. Foner, High-field antiferromagnetic resonance in Cr_2O_3, *Phys. Rev.*, 1963, **130**(1), 183–197.

66 C. G. Schull, W. A. Strauser and E. O. Wollan, Neutron diffraction by paramagnetic and anti-ferromagnetic substances, *Phys. Rev.*, 1951, **83**(2), 333–345.

